Supporting Information

All-Color Subwavelength Output of Organic Flexible Microlasers

Yuanchao Lv,[†,§] Yong Jun Li,[*,†] Jing Li,[‡] Yongli Yan,[†] Jiannian Yao,[†,§] and Yong Sheng Zhao[*,†,§]

[†]*Key Laboratory of Photochemistry, Institute of Chemistry, Chinese Academy of Sciences, Beijing 100190, China.*

[‡]*Key Laboratory of Photochemical Conversion and Optoelectronic Materials, Technical Institute of Physics and Chemistry, Chinese Academy of Sciences, Beijing 100190, China.*

[§]*University of Chinese Academy of Sciences, Beijing 100049, China.*

E-mail: yongjunli@iccas.ac.cn; yszhao@iccas.ac.cn

Contents

Materials, calculation methods and experimental details

1. Materials

The 2,5-diphenyl-1,4-distyrylbenzene with two trans double bonds (*trans*-DPDSB), 1,4-bis(α-cyano-4-diphenylaminostyryl)-2,5-diphenylbenzene (CNDPASDB), and 3-[4-(dimethylamino)phenyl]-1-(2-hydroxy-4-methoxyphenyl)-2-propen-1-one (HMDMAC) was synthesized according to the reference.[1-3] The polystyrene (PS, M.W. 250,000),silver nitrate ($AgNO_3$), polyvinylpyrrolidone (PVP), Coumarin-153 (C153)and ethylene glycol (EG) were purchased from Aldrich Chemical Co., and used without further purification. The AgNWs were synthesized by reducing $AgNO_3$ with ethylene glycol (EG) in the presence of PVP.

2. Preparation of the organic microdisk/AgNW heterostructures

In a typical preparation, a small amount of ultrapure water (10-50 μL) was added into 1 mL PS/DMF solution (10 mg/mL), which was subsequently treated with sonication for 30 s. After that, a drop of asprepared mixed solution (5 μL) was drop-cast onto a glass slide, and at the same time the AgNW solution (10 μL) in DMF was dropped on the same glass slide. Another glass substrate was immediately covered to form the tiny gap as a template for the self-assembly. With the gradual evaporation of the solvent, the capillary force induced AgNWs to connenct with the microdisks, and the AgNWs were partially embedded in the microdisks. The AgNW connected microdisks were obtained on the substrate after the complete volatilization of DMF. The organic dyes were added to the polymer solution at a concentration of ~1 wt% relative to PS. The AgNW connected dual-color microdisks were synthesized by simultaneously adding 0.1 mg CNDPASDB and 0.7 mg trans-DPDSB molecules into the polymer solution (1 mL) before undergoing the steps mentioned above.

3. Calculation method

In the simulation, the output coupling efficiencies (η) were obtained by calculating the power flow (P) around the AgNW and the total electromagnetic wave energy inside the cavity (I). The power flow is in accordance with the power of light guided by surface plasmon modes. The total radiation power of the cavity can be obtained as Iω/Q, where ω is the cavity mode frequency, Q is the quality factor of the mode. The output coupling efficiencies to the surface plasmon modes were obtained as $\eta = P/(I\omega/Q)$.[4]

4. Characterization

The morphology of the AgNW connected microdisk was examined with scanning electron microscopy (FEI Nova NanoSEM450). The absorption and fluorescence spectra were measured on a UV-visible spectrometer (Perkin-Elmer Lambda 35) and a fluorescent spectrometer (Hitachi F-7000), respectively.

Bright-field optical images and fluorescence microscopy images were taken from an inverted fluorescence microscope (Nikon Ti-U), by exciting the samples with a mercury lamp. The single AgNW connected microdisk was uniformly excited by a focused pulse laser beam (355 nm, 400 nm, 150 fs, 1000 Hz). The spatially resolved spectra were measured with a monochrometer (Princeton Instrument Acton SP 2300i) connected with an EMCCD (Princeton Instrument ProEM 1600B). Polarization profiles of the emission intensity were obtained by setting a polarizer in front of the detector.

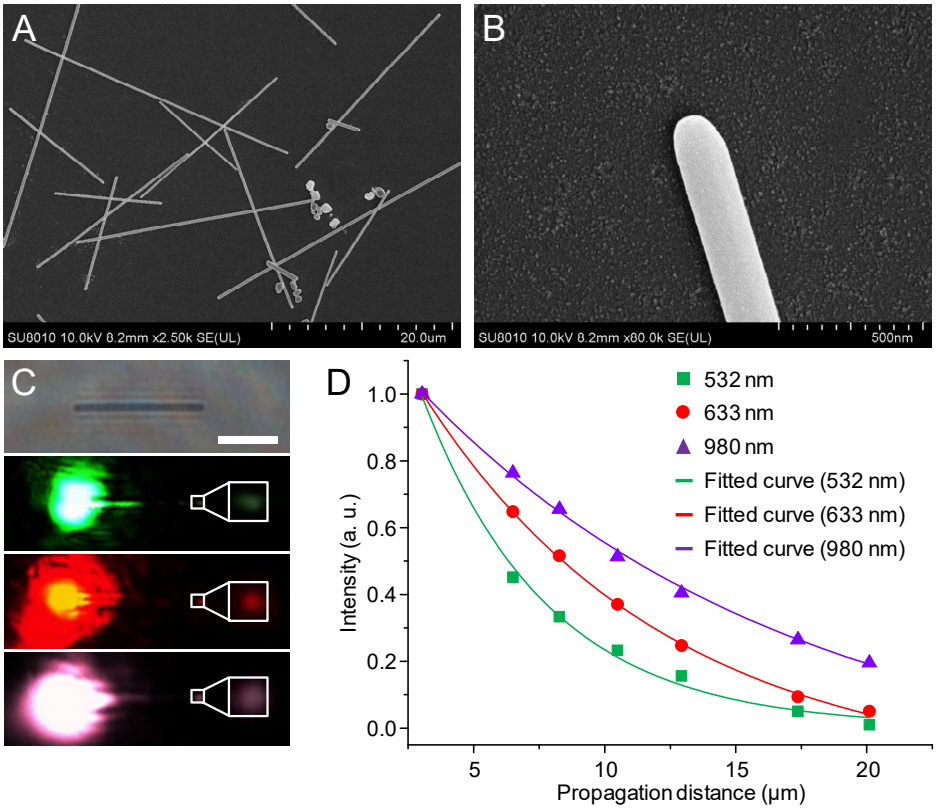

Figure S1. The morphology and optical property of the chemically synthesized AgNWs. (A) Image of massive AgNWs that were synthesized by reducing $AgNO_3$ with ethylene glycol in the presence of polyvinylpyrrolidone. (B) Image of the AgNW with larger magnification. (C) Optical microscopy images of a typical AgNW irradiated by focused laser beams at the wavelength of 532 nm, 635 nm and 980 nm, respectively. Bright points magnified in the white boxes are the results of SPPs scattering from the AgNW distal ends. Scale bar is 5 μm. (D) The relative intensity $I(x)/I_0$ versus the propagation distance at the wavelength of 532 nm, 633 nm and 980 nm.

The atomically smooth surfaces of the chemically synthesized AgNWs would help to reduce the total surface plasmon propagation loss in a wide spectral range (Figure S1A and S1B).[5] Here, seven representative AgNWs with lengths ranging from 3.2 to 20.1 μm and diameters of 170 ± 10 nm were utilized to investigate the propagation loss. The SPPs in AgNWs were launched by focusing laser beams (532 nm, 635 nm and 980 nm) at one distal end of the AgNW (Figure S1C). The bright point observed from the other end (magnified in the white boxes) indicates the formation of typical SPPs waveguide. The intensities of both the scattered light at the excitation spots (I_0) and the scattered SPPs

at the opposite distal ends ($I(x)$) were collected to calculate the propagation length (L_0) and the propagation loss (α) of the SPPs in the AgNW. It is noted that L_0 is the propagation length over which the intensity of SPPs decreases to $1/e$ the initial values. The relative intensity $I(x)/I_0$ versus the propagation distance shown in Figure S1D was fitted by the equation

$$\frac{I(x)}{I_0}=e^{-x/L_0} \quad (1),$$

where x is the distance between the excitation spot and the SPPs scattering point at the AgNW distal end. The propagation loss (α) is inversely proportional to the propagation length (L_0) as

$$\alpha=\frac{-10\times\log(1/e)}{L_0} \quad (2).$$

The SPPs propagation lengths in these chemically synthesized AgNWs were obtained as 4.79 μm (532 nm), 9.27 μm (635 nm), and 14.3 μm (980 nm), and the corresponding propagation losses were 0.91 dB/μm (532 nm), 0.46 dB/μm (635 nm), and 0.31 dB/μm (980 nm), which agree well with the previously reported results.[6,7] Such low propagation loss of the AgNW is attributed to the atomically smooth surface, which enables the AgNW to support the SPPs in the full visible range.

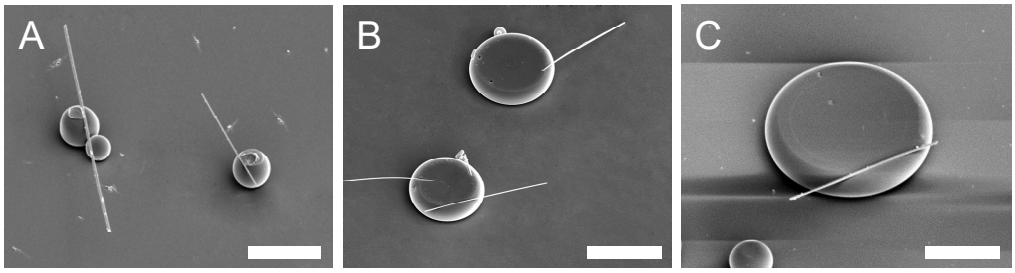

Figure S2. SEM images of the organic microdisk/AgNW heterostructures with different sizes. When the amount of water added into the PS solutions (1 mL) was adopted as 10, 20, and 30μL, the microdisks with different diameters were finally obtained as ~4 μm (A), 10 μm (B) and 20 μm (C), respectively.

The diameter of the organic microdisk was tuned from ~4 to 20 μm by changing the amount of water added from 10 to 30 μL, which could be utilized to modulate the WGM lasers and the subwavelength output.

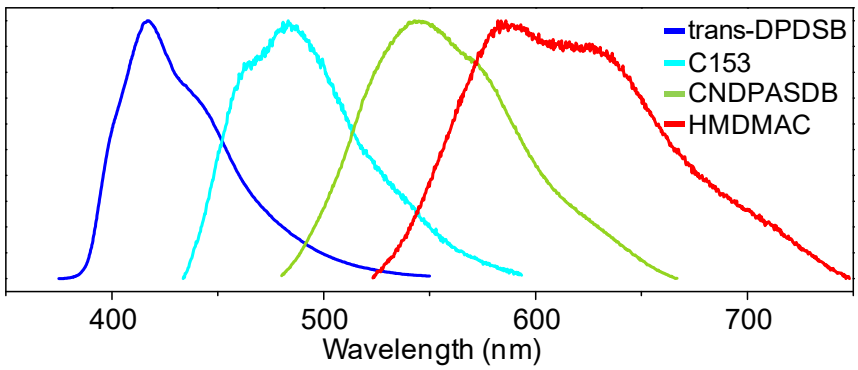

Figure S3. Emission spectra of the four laser dyes (trans-DPDSB, C153, CNDPASDB and HMDMAC) in PS.

The photoluminescence spectra of the four laser dyes (trans-DPDSB, C153, CNDPASDB and HMDMAC) in PS span the full visible spectrum, offering an opportunity to achieve the all-color subwavelength output.

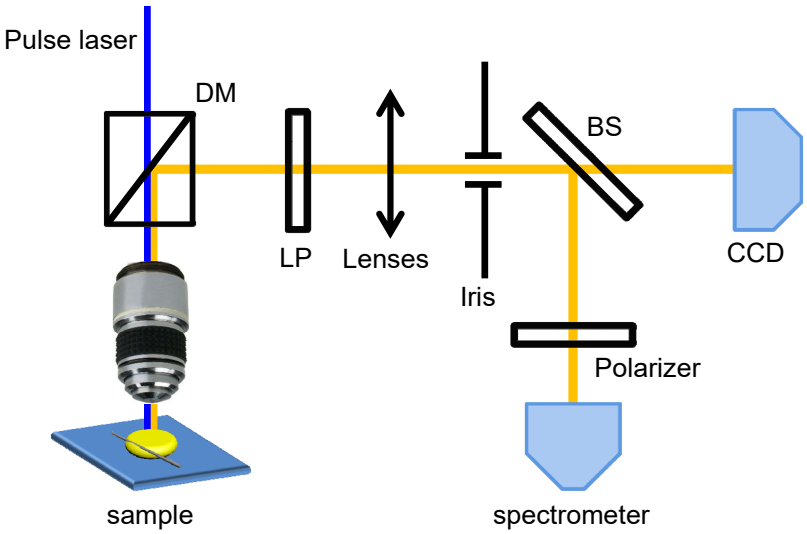

Figure S4. Schematic demonstration of the experimental setup for the optical characterization.

A homemade micro-photoluminescence system was used to exam the optical properties of the composite microdisk. A focused pulse laser beam (355nm, 400nm, 150 fs, 1000 Hz) was used to pump the organic/silver composite microdisks. The microdisk resonators were dispersed on a glass substrate (refractive index about 1.5). An objective lens (50×, numerical aperture 0.8) was used to focus the pump beam to a 1-μm-diameter spot on the edge of the disk vertically. The PL signal was collected by the same microscope objective, passed through the dichroic mirror (DM 400 nm), then a longpass emission filter (400 nm, 420 nm) to eliminate the exciter light, focused by a group of lenses onto a confocal iris. The output signal can be spatially selected by the iris and recorded using a spectrometer. By rotating the polarizer in front of the detector, the polarization of the light signal can be obtained.

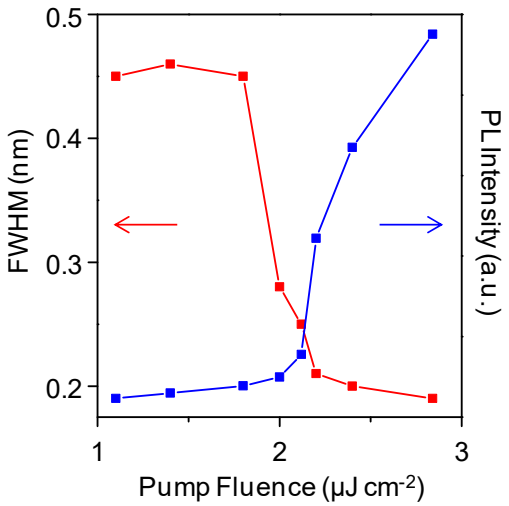

Figure S5. Plots of Photoluminescence (PL) peak intensities (blue line) and FWHM (red line) *vs* the pump fluence.

Figure S5 depicted the PL intensity and the full width at half-maximum (FWHM) at 579 nm as a function of the pump fluence, showing a threshold characteristic at ~2.1 μJ/cm^{-2}.Above the onset power, the peak intensity increased rapidly with the pump fluence, and the FWHM dramatically decreased down to ~0.19 nm, which revealed the stimulated emission of the doped organic dye.

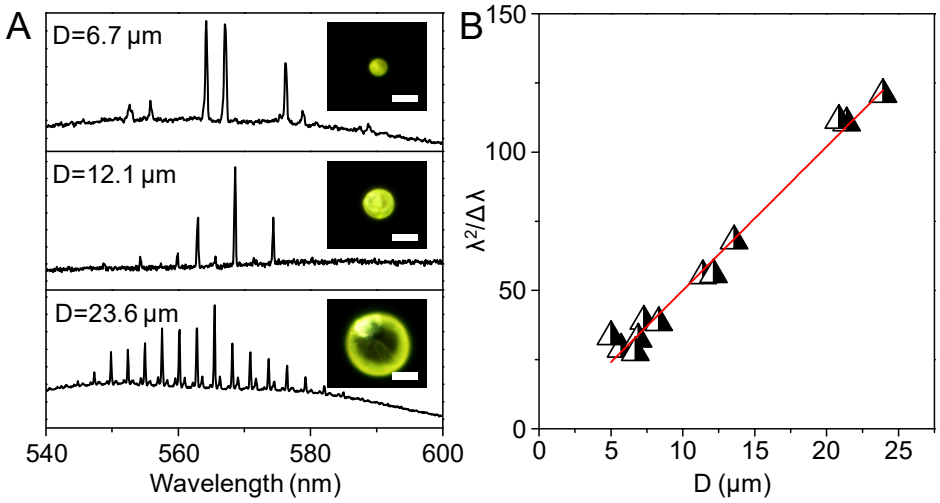

Figure S6. Microcavity effect of the composite microdisks. (A) PL spectra of microdisks with different diameters and corresponding PL images. Scale bars are 5 μm. (B) Relationship between$\lambda^2/\Delta\lambda$ and the diameter of the microdisk. The red line is a fit to the function $\lambda^2/\Delta\lambda = n\pi D$.

The lasing spectra of microdisks with different diameters were measured, which presented an increasing number of modes with increasing the diameter of the microdisk. According to the WGM theory, the mode spacing, $\Delta\lambda$, and the cavity length, L, would satisfy the equation $\lambda^2/\Delta\lambda = n\pi D$, where λ is the wavelength of the guided light, $\Delta\lambda$ is the mode spacing, n is the group refractive index and D is the cavity length. The plot of $\lambda^2/\Delta\lambda$ versus D demonstrated clearly a linear relationship, indicating that the lasing mechanism was ascribed to WGM resonance.[8]

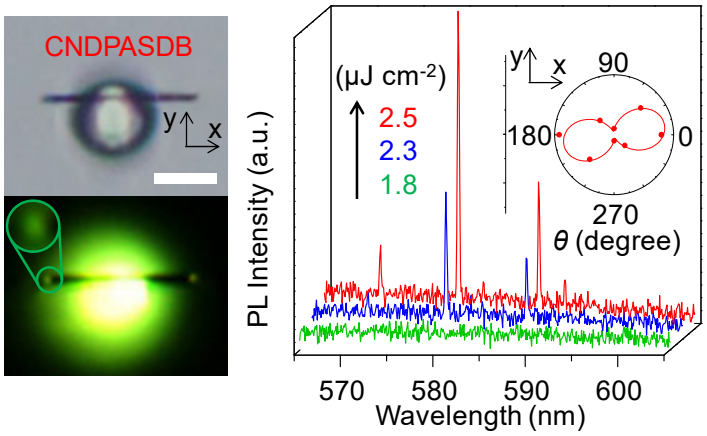

Figure S7. PL spectra collected from the left tip of the AgNW in Figure 3A as a function of the pump fluence. Insets: polarization profiles of the emission intensities of the lasing modes.

The SPPs were efficiently launched and scattered back as photons from the left tip of the AgNW. The emission spectra collected from the left tip showed the same optical modes as compared with that obtained at the WGM microdisk edge and the right tip. Moreover, the polarizing characteristic of the light outputted from the left tip was also consistent with that of the microcavity modes, i.e., the corresponding optical modes (579 nm) were polarized parallel to the AgNW. Therefore, the emission spectra collected from the two AgNW tips showed the same optical characteristic.

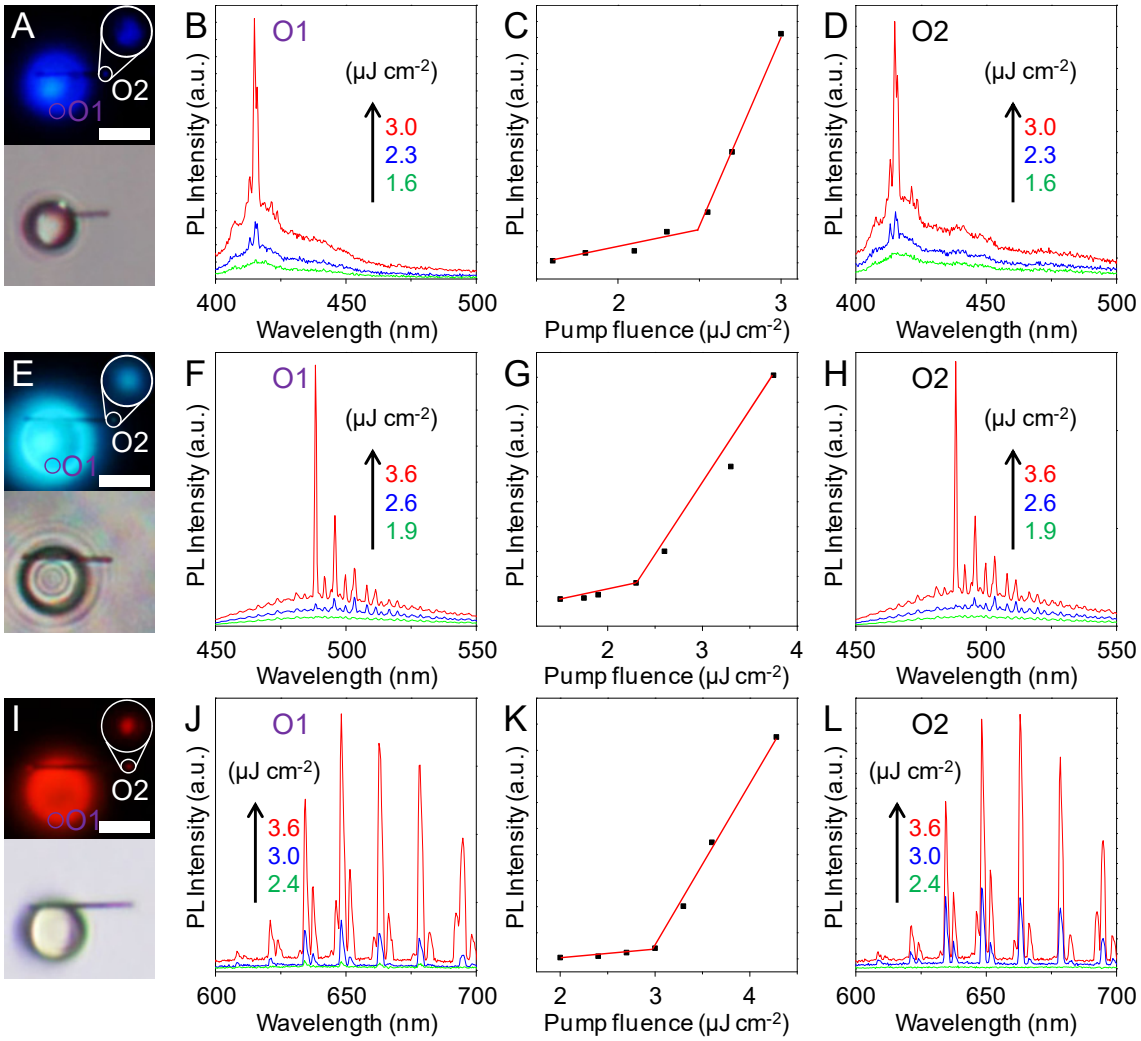

Figure S8. Lasing behaviors of the organic/silver composite microdisks doped with trans-DPDSB, C153 and HMDMAC, respectively. (A, E, I) Bright-field and PL images of the organic/silver composite microdisks doped with trans-DPDSB (A), C153 (E), and HMDMAC (I)uniformly excited by a focused pulse laser beam (355nm (A), 400nm (E), 400 nm(I)). Luminescent points magnified in white circles are the result of scattering of SPPs from the AgNW tips. O1 and O2 denote the spectra collection positions at the microdisk edge and AgNW tips, respectively. Scale bars are 5 μm. (B, F, J) Spectra collected from the microdisk edge. (C, G, K) Plots of the PL peak intensity vs the pump fluence. (D, H, L) Spectra collected from the AgNW tips.

The trans-DPDSB, Coumarin-153, HMDMAC, each with distinct gain region, were doped into the flexible resonant cavities as gain media. The composite microdisk doped with trans-DPDSB was pumped by a 355 nm focused pulse laser beam. The other two samples (C153, HMDMAC) were pumped by a 400 nm focused pulse laser beam. With increasing pump fluence, the intensity of the PL peaks (trans-DPDSB 415 nm, C153 488 nm, HMDMAC 648 nm) in the corresponding gain regions were all dramatically amplified. The pump fluence dependence of the PL intensities showed a nonlinear threshold behavior (trans-DPDSB ~2.5 μJ cm^{-2}, C153 ~2.3 μJ cm^{-2}, HMDMAC ~3 μJ cm^{-2}). The optical microscopy images exhibited blue, cyan and red laser emissions, and the corresponding output from the AgNW tips *via* SPPs could be clearly observed. The PL spectra collected from the AgNW tips indicated that all color subwavelength output could be realized in the organic/silver composite microdisks by doping with various laser dyes.

References

(1) Li, Y.; Shen, F.; Wang, H.; He, F.; Xie, Z.; Zhang, H.; Wang, Z.; Liu, L.; Li, F.; Hanif, M.; Ye, L.; Ma, Y. *Chem. Mater.* **2008**, *20*, 7312.

(2) Xie, Z.; Wang, H.; Li, F.; Xie, W.; Liu, L.; Yang, B.; Ye, L.; Ma, Y. *Cryst. Growth Des.* **2007**, *7*, 2512.

(3) Cheng, X.; Wang, K.; Huang, S.; Zhang, H.; Zhang, H.; Wang, Y. *Angew. Chem. Int. Ed.* **2015**, *54*, 8369.

(4) Li, Y. J.; Lv, Y.; Zou, C.-L.; Zhang, W.; Yao, J.; Zhao, Y. S. *J. Am. Chem. Soc.* **2016**, *138*, 2122.

(5) Ditlbacher, H.; Hohenau, A.; Wagner, D.; Kreibig, U.; Rogers, M.; Hofer, F.; Aussenegg, F. R.; Krenn, J. R. *Phys. Rev. Lett* .**2005**, *95*, 257403.

(6) Yan, R.; Pausauskie, P.; Huang, J.; Yang, P. *Proc. Natl. Acad. Sci. U. S. A.* **2009**, *106*, 21045.

(7) Ma, Y.; Li, X.; Yu, H.; Tong, L.; Gu, Y.; Gong, Q. *Opt. Lett.* **2010**, *35*, 1160.

(8) Wei, C.; Liu, S.-Y.; Zou, C.-L.; Liu, Y.; Yao, J.; Zhao, Y. S. *J. Am. Chem. Soc.* **2015**, *137*, 62.